NATIONAL ADVISORY COMMITTEE FOR AERONAUTICS

TECHNICAL NOTE

No. 1313

AN INVESTIGATION OF THE EFFECT OF BLADE CURVATURE ON CENTRIFUGAL-IMPELLER PERFORMANCE

By Robert J. Anderson, William K. Ritter
and Dean M. Dildine

Flight Propulsion Research Laboratory
Cleveland, Ohio

Washington
May 1947

NATIONAL ADVISORY COMMITTEE FOR AERONAUTICS

TECHNICAL NOTE NO. 1313

AN INVESTIGATION OF THE EFFECT OF BLADE CURVATURE ON CENTRIFUGAL-IMPELLER PERFORMANCE

By Robert J. Anderson, William K. Ritter
and Dean M. Dildine

SUMMARY

Three centrifugal impellers, the same except for angular blade curvature, were investigated to determine the effect of the distribution of blade loading on impeller performance. The blade curvatures are geometrically definable shapes and the differences in blade loading were compared on the basis of particle travel with constant axial velocity along the blade surface. Impeller A has a parabolic blade curvature and a constant blade loading. Impeller B has an elliptical blade curvature with a loading that decreases with increasing impeller depth and that has a higher initial value than that of impeller A. Impeller C has a circular blade curvature with the highest initial blade loading, which also decreased with increasing impeller depth. The blade curvatures of impellers A and B extend the full depth of the impellers; the blade curvature of impeller C extends 0.60 of the impeller depth. The blades of impeller C have a 7.5° forward inclination at the impeller discharge. The three impellers were investigated with a vaneless diffuser in a variable-component compressor test rig with the same conditions and instrumentation.

Impeller B had the highest peak adiabatic efficiency at all equivalent tip speeds except 1400 and 1600 feet per second. Impeller C had the lowest peak adiabatic efficiency of all three impellers at equivalent tip speeds above 1000 feet per second but the largest slip factor of all three impellers at all equivalent tip speeds. The variation of pressure ratio at peak adiabatic efficiency with equivalent tip speed was more nearly the same for the three impellers than the variation of slip factor and peak adiabatic efficiency. Impeller C had the largest maximum specific capacity at all speeds; impeller B had nearly the same maximum specific capacity as impeller C; and impeller A had from 6 to 11 percent lower maximum specific capacity than impeller C. Impeller B had the largest operating range above an adiabatic efficiency of 0.70 at a pressure ratio of 1.80, and impeller A had the largest

operating range above an adiabatic efficiency of 0.70 from pressure ratios of 2.20 to 3.00. Impeller C had the smallest operating range above 0.70 adiabatic efficiency at all pressure ratios between 1.80 and 3.00.

INTRODUCTION

An investigation has been made of the performance of three centrifugal-type impellers to determine the effect of three different distributions of blade loading on the efficiency, the pressure ratio, the flow capacity, and the range. The three impellers have the same inner and outer diameters and the same distributions of curvature over the front and rear shrouds. The leading edges of the three impellers were designed to have shockless entry at the same air flows and impeller speeds. The variations in blade loading were achieved by different distributions of the curvature of the cylindrical surfaces generating the blades. These impellers, being of the same external geometry, were tested in the same installation.

This investigation is a continuation of the research presented in references 1 and 2. The scope of the investigation reported in these reports, however, was limited to that type of impeller in which the angular velocity of the air is accelerated to the angular velocity of the impeller before any appreciable compression by centrifugal force is allowed. The blade loading in the inlet section, or inducer, is thus high, owing to the large angular accelerations imparted to the air. As the flow proceeded through the inlet section, the angular velocity of the air approached that of the impeller, and the blade loading suddenly decreased.

It was feared that this sudden reduction in blade loading at the end of the inlet section caused irretrievable pressure losses resulting from flow separation. These losses can be lessened or even prevented by insuring that no sensible reduction in angular acceleration occurs before the Coriolis acceleration, resulting from an increase in the radius of rotation, is well developed.

The curvature of the blade surfaces for one of the impellers of the present investigation is of the same type as those of the inducers reported in reference 1. The curvature is distributed continuously throughout the entire depth of the impeller; and, at each point within the impeller, angular and Coriolis accelerations were simultaneously imparted to the air. The curvature of the front and rear shrouds was designed to avoid any abrupt changes in blade loading. The other two impellers were designed to have successively increasing blade loadings near the impeller inlet.

This report presents a comparison of the performance of the three impellers over a range of tip speeds and volume flows. The performance characteristics compared include the efficiency, the slip factor, the maximum flow capacity, the range of flow, and the pressure ratio.

IMPELLER DESIGN

Each of the three impellers used in this investigation has 18 blades, the same blade-entrance angles, and the same entrance and discharge diameters. The blade-entrance angle is defined as the complement of the acute angle between blades at the entrance edge and a plane perpendicular to the axis of rotation. The blade-entrance angle for each of these impellers is 60° at the blade tip and the tangent of the angle varies linearly with impeller radius.

An axial-plane section for the three impellers (A, B, and C), with the pertinent dimensions given, is shown in figure 1. Impellers A and B have a radial entrance edge and impeller C has an entrance edge that deviates from the others as shown by the dotted line in figure 1. The indicated difference in the entrance edge of impeller C from that of impellers A and B is the result of the necessity for keeping the entrance angles of all three impellers the same at all radii. The entrance edges of all three impellers were sharpened to a maximum radius of 0.024 inch. Front views of impellers A, B, and C are shown in figure 2.

The blade curvature of impeller A is illustrated in figure 3. Figure 3(a) shows a cylindrical section that has a diameter equal to the outside diameter of the impeller and a length equal to the axial length of the impeller. The blade surface (shaded) consists of radial elements and the intersection of the cylinder with the blade surface defines the blade curvature. The portion of the blade surface used by the impeller is shown in figure 3(b). The bounding axial-plane curvatures were chosen to prevent excessive adverse pressure gradients at equivalent tip speeds below 1200 feet per second.

The passage area, taken perpendicular to a mean-flow-path line formed by rotating each radial blade element into an axial cross-sectional plane of the impeller, was constant.

The blade curvature of impeller A (fig. 2(a)) corresponds to that of a parabola on the developed surface of the cylinder. This

curvature extends the full depth of the impeller and is so oriented that a particle following the blade with a constant axial velocity would have a constant angular acceleration. The blade curvature of impeller A is nearly the same as that of the 4-inch inducer of reference 1.

The blade curvature of impeller B (fig. 2(b)) was formed in the same manner as that of impeller A but, for impeller B, the blade curvature corresponds to an ellipse on the developed cylindrical surface. This curvature also extends the full depth of the impeller. A particle following the blade of impeller B would have a higher initial value of angular acceleration than a particle following the blade of impeller A, and it would have a decreasing rate of angular acceleration as it progressed through the impeller.

The blade surface of impeller C was formed in a different manner from the blade surfaces of impellers A and B. The blade elements are nonradial but are inclined in the direction of rotation $7\frac{1}{2}^{\circ}$ to a radial line at the impeller discharge. The inlet portion of the blade surfaces for the first 60 percent of the impeller axial depth generates a circular cylinder and the remainder of the blade surface generates a plane tangent to the circular cylinder. A particle following the blade with a constant axial velocity would have a higher initial value of angular acceleration than a particle following the blade of impeller A or B, and it would have a decreasing angular acceleration as it progressed through the impeller.

When the air is assumed to flow along the surface of the impeller blades (the assumption of an infinite number of blades), the rate of pressure increase at the entrance, owing to the increase in angular velocity, would be lowest for impeller A and increase in the order A, B, and C for the three impellers. For the configuration of the three impellers and the assumption of an infinite number of blades, the average angular velocity leaving the impeller would be highest for impeller C and lowest for impeller A. At the discharge the air velocity of impellers A and B would be the same at the maximum impeller depth, but at all other points at the discharge the air velocity of impeller B would be higher than that of impeller A.

APPARATUS AND PROCEDURE

Test Rig

A variable-component compressor test rig conforming to the recommendations of reference 3 was used for this investigation. A

schematic view of this apparatus is shown in figure 4. The collector casing is enclosed in an insulating box, the walls of which are composed of one-quarter inch of hard asbestos, 1 inch of insulating board, and one-half inch of plywood. The impellers were driven with a 1500-horsepower induction motor through a step-up gear. The collector casing was mounted separately from the gear box to reduce heat transfer between it and the gear drive. The arrangement of the equipment is shown in figure 5.

The impellers were tested in conjunction with a 24-inch-diameter vaneless diffuser of constant area. Every component part except the impeller was the same for all tests.

Instrumentation

The equipment was instrumented with thermocouples and pressure taps and tubes located in conformance with reference 3. This instrumentation provides an entrance measuring station 2 pipe diameters upstream of the impeller, and two discharge measuring stations 12 pipe diameters downstream of the collector casing. In addition to the standard instrumentation, pressure and temperature measurements were taken at the diffuser discharge. Three shielded total-pressure rakes composed of five tubes each were equally spaced around the diffuser circumference for the pressure measurements. These rakes were insensitive to angle of yaw up to $\pm 44^{\circ}$. Two calibrated thermocouples were placed midway between the front and rear diffuser surfaces 180° apart for the temperature measurement. These thermocouples were a high-recovery type, insensitive to angle of yaw up to $\pm 20^{\circ}$ and similar to the Pratt & Whitney probe described in reference 4. The total pressures and temperatures measured at the diffuser discharge were used for the comparative performance of the impellers in this investigation.

Each impeller is charged with the pressure loss that occurs in the diffuser but not with the loss in dynamic pressure that occurs in the large collector chamber. The temperature measurement at the diffuser discharge was used because it has been found that this procedure allows the performance to be correlated at all inlet-air temperatures, whereas the performance based upon discharge-pipe temperatures does not correlate at all inlet-air temperatures. At ambient inlet-air temperatures, the efficiencies based on the diffuser-discharge temperatures were as much as 0.04 lower than those based on temperatures measured in the discharge pipe.

Procedure

All three impellers were investigated with atmospheric and refrigerated inlet air in accordance with references 3 and 5. For each test the equivalent tip speed was held constant and the volume flow was varied in steps from maximum flow to heavy pulsation. At all points except that for the lowest pressure ratio at maximum flow, a discharge pressure of 39.50 inches of mercury absolute was maintained. The range of equivalent tip speeds was 900 to 1600 feet per second for impellers A and B, and 800 to 1500 feet per second for impeller C.

SYMBOLS

The symbols used in this report are listed here for convenience:

D_2	impeller-discharge diameter, feet
$p_{t,1}$	inlet stagnation pressure, inches of mercury absolute
$p_{t,2}$	discharge stagnation pressure, inches of mercury absolute
$p_{t,2}/p_{t,1}$	pressure ratio
$Q_{t,1}$	volume flow based on inlet stagnation conditions, cubic feet per minute
$Q_{t,1}/\sqrt{\theta}\ D_2^2$	specific capacity corrected to sea-level conditions, cubic feet per minute per square foot
$T_{t,1}$	inlet stagnation temperature, $^{\circ}R$
U	actual impeller tip speed, feet per second
$U/\sqrt{\theta}$	equivalent tip speed; actual tip speed corrected to sea-level conditions
η_{ad}	adiabatic temperature-rise ratio or adiabatic efficiency
θ	ratio of actual inlet stagnation temperature to standard NACA sea-level temperature

RESULTS AND DISCUSSION

Impeller Efficiency

The variation of peak adiabatic efficiency with equivalent tip speed for the three impellers is compared in figure 6. At an equivalent tip speed of 900 feet per second, impeller A had a peak adiabatic efficiency of 0.78, and the peak adiabatic efficiency decreased to 0.77 at an equivalent tip speed of 1100 feet per second, to 0.69 at 1400 feet per second and to 0.56 at 1600 feet per second. The rate of change in peak adiabatic efficiency was greatest between equivalent tip speeds of 1400 and 1500 feet per second for impeller A.

At an equivalent tip speed of 900 feet per second, impeller B had a peak adiabatic efficiency of 0.82 and the peak adiabatic efficiency decreased to 0.78 at an equivalent tip speed of 1100 feet per second, to 0.67 at 1400 feet per second, and to 0.53 at 1600 feet per second. The rate of change in peak adiabatic efficiency for impeller B was greatest between equivalent tip speeds from 1300 to 1400 and from 1500 to 1600 feet per second.

At an equivalent tip speed of 800 feet per second, impeller C had a peak adiabatic efficiency of 0.80 and the peak adiabatic efficiency decreased to 0.75 at an equivalent tip speed of 1100 feet per second, to 0.59 at 1400 feet per second, and to 0.54 at 1500 feet per second. The peak adiabatic efficiency of impeller C decreased abruptly between equivalent tip speeds of 1200 and 1300 feet per second.

Impeller B, with the elliptical blade curvature, had the highest peak adiabatic efficiency at all equivalent tip speeds except 1400 and 1600 feet per second. Impeller A, with the parabolic blade curvature, decreased in peak adiabatic efficiency at approximately the same rate as impeller B, and the greatest difference between the peak adiabatic efficiency of the two impellers was 0.04 at an equivalent tip speed of 900 feet per second. At equivalent tip speeds of 1400 and 1600 feet per second, impeller A had the highest peak adiabatic efficiency of the three impellers. Impeller C, with the circular blade curvature, had the lowest peak adiabatic efficiency at equivalent tip speeds higher than 1000 feet per second. Up to an equivalent tip speed of 1200 feet per second, the peak adiabatic efficiency of impeller C was no more than 0.03 lower than that of impeller B, but at equivalent tip speeds of 1300 feet per second and higher, the peak adiabatic efficiency of impeller C was 0.08 to 0.10 below that of impeller B.

Energy Addition and Pressure Ratio

A comparison of the slip factors at peak adiabatic efficiency of the three impellers over the range of equivalent tip speeds is shown in figure 7. The slip factor is defined as the ratio of the energy imparted to the air to the energy that would be imparted if the air were discharged with a tangential velocity component equal to the peripheral velocity of the impeller. This factor is proportional to the actual energy addition imparted to the air by each impeller. Impeller C consistently had the highest slip factor of all three impellers and therefore the highest actual energy addition at all equivalent tip speeds. Impeller A had the lowest slip factor at all equivalent tip speeds and therefore the lowest actual energy addition. This order is in agreement with that previously determined from a consideration of the impeller designs. The slip factors of impellers A and B were much closer to each other than either of them was to the slip factor of impeller C. The slip factors of all three impellers tended to increase with equivalent tip speed.

The pressure ratios at peak adiabatic efficiency for the three impellers are compared at various equivalent tip speeds in figure 8. For each of the three impellers, the pressure ratio for the peak adiabatic efficiency at a given equivalent tip speed was within 1 percent of the corresponding peak pressure ratio. Impeller C had the highest pressure ratio at all equivalent tip speeds up to 1200 feet per second. The pressure ratio varied from 1.91 at 900 feet per second up to 2.72 at 1200 feet per second. Impeller B had the second-highest pressure ratio at all equivalent tip speeds up to 1200 feet per second, with a pressure ratio of 1.82 at 900 feet per second up to a pressure ratio of 2.61 at 1200 feet per second. Impeller A had the lowest pressure ratio over the range of equivalent tip speeds from 900 to 1300 feet per second, with a pressure ratio of 1.77 at 900 feet per second and a pressure ratio of 2.50 at 1200 feet per second.

Up to an equivalent tip speed of 1200 feet per second, the pressure ratios of all three impellers increased with equivalent tip speed at approximately the same rate and the relation between the pressure ratios of the three impellers was unchanged. At equivalent tip speeds higher than 1200 feet per second, the relation between the pressure ratios of the three impellers changed frequently. At an equivalent tip speed of 1300 feet per second, the pressure ratio at peak adiabatic efficiency of impellers A, B, and C was 2.85, 2.92, and 2.87, respectively; at 1400 feet per second, it was 3.21, 3.13, and 3.05, respectively; at 1500 feet per second, it was 3.21, 3.37, and 3.21, respectively.

The rate of increase in pressure ratio with equivalent tip speed dropped to zero for impeller A between 1400 and 1500 feet per second; it decreased in value for impeller C at 1200 feet per second; and it dropped off increasingly at equivalent tip speeds above 1300 feet per second for impeller B. The variation of pressure ratio at peak adiabatic efficiency with equivalent tip speed was more nearly the same for the three impellers than was the variation of slip factor or peak adiabatic efficiency with equivalent tip speed.

Flow Characteristics

The maximum specific capacity increased with increasing equivalent tip speed at nearly the same rate for all three impellers (fig. 9). Impeller C had the highest maximum specific capacity, which varied from 6850 to 7925 cubic feet per minute per square foot at equivalent tip speeds from 800 to 1500 feet per second, respectively. Impeller B, which had nearly the same maximum specific capacity as impeller C, varied from 6650 to 7904 cubic feet per minute per square foot at equivalent tip speeds from 800 to 1500 feet per second, respectively, and to 7984 cubic feet per minute per square foot at 1600 feet per second. Impeller A had the smallest maximum specific capacity, which varied from 6100 to 7500 cubic feet per minute per square foot at equivalent tip speeds from 800 to 1600 feet per second, respectively. Impeller C with the highest initial blade loading had the highest maximum specific capacity of the three impellers and impeller A with the lowest initial blade loading had the lowest with a maximum specific capacity 6 to 11 percent smaller than that of impeller C.

Operating Range

The performance characteristics of impellers A, B, and C are presented in figure 10, where the pressure ratios at each equivalent tip speed are plotted against specific capacity. Contour lines of constant adiabatic efficiency are also shown on these figures. For a comparison of the performance of these impellers, the useful operating range is defined as the range of specific capacity in which the adiabatic efficiencies are greater than 0.70. These operating ranges are determined from figure 10. The useful operating range at any constant pressure ratio will lie within the 0.70 adiabatic-efficiency lines or be limited on the minimum end by the occurrence of surge. The operating ranges at adiabatic efficiencies above

0.70 for pressure ratios of 1.80, 2.20, 2.60, and 3.00 for impellers A, B, and C follow:

Pressure ratio	Specific capacities at upper and lower limit of operating range		
	Impeller A	Impeller B	Impeller C
1.80	2800-6200	3000-6700	4750-6500
2.20	3800-6500	4500-7050	5500-6750
2.60	4700-6700	5400-7150	6250-6650
3.00	5750-6700	----------	----------

At a pressure ratio of 1.80, impeller B had the greatest operating range of all three impellers but, at pressure ratios of 2.20 and above, impeller A had the greatest operating range. Impeller C had a much smaller operating range than either impeller A or B at pressure ratios from 1.80 to 3.00. Neither impeller B nor C had adiabatic efficiencies as high as 0.70 at a pressure ratio of 3.0.

At equivalent tip speeds of 1400 and 1500 feet per second, the closure of the throttles that varied the specific capacity was limited by surge for all three impellers; the specific capacity at surge was therefore nearly the same as the maximum specific capacity, which resulted in virtually no definable operating range at these speeds. Impeller B exhibited an operational instability near the maximum specific capacity at equivalent tip speeds higher than 1300 feet per second and impeller C, a similar instability at 1200 and 1300 feet per second. The parameters of pressure ratio and specific capacity are inadequate to describe the impeller performance in this instability region when several speeds are plotted on the same figure. The highest four speeds of impellers B and C are plotted separately in figures 11 and 12, respectively, on the specific-capacity and pressure-ratio parameters; the dashed lines show the extent of the operational instability, which was characterized by low-frequency, high-amplitude pulsations of the inlet and discharge pressures and by inflection points on the performance curves. The data in the region of operational instability were taken at points relatively free from pressure pulsation.

An impeller tested at the Cleveland laboratory was also found to have virtually no definable operating range at high speeds. With the aid of a surge inhibitor, a stable operating range was found at higher pressure ratios than those at which surge occurred without the inhibitor. The surge inhibitor provided a means of passing through

an unstable operating region that was similar in many respects to the unstable operating regions encountered with impellers B and C. Probably stable operating ranges at pressure ratios higher than those limited by surge also exist for the impellers of this investigation. Both the operational instability and the lack of an appreciable operating range occurred only at high equivalent tip speeds; the velocity gradients along the mean flow path of the impeller at these speeds were greater than the maximum value assumed in the design of the passage area of these impellers.

SUMMARY OF RESULTS

An investigation of the effect of angular curvature, or rate of adding angular velocity, of impeller blades has shown for the three blade forms tested:

1. Impeller B, with the elliptical blade curvature, had the highest peak adiabatic efficiency at all of the equivalent tip speeds except 1400 and 1600 feet per second. Impeller A, with the parabolic blade curvature, had the highest peak adiabatic efficiency at equivalent tip speeds of 1400 and 1600 feet per second. Impeller C, with the circular blade curvature, had the lowest peak adiabatic efficiency at equivalent tip speeds higher than 1000 feet per second. For the range of tip speeds investigated, all three impellers decreased in adiabatic efficiency with increasing tip speed.

2. Impeller C had the highest slip factor of all three impellers.

3. The variation of pressure ratio at peak adiabatic efficiency with equivalent tip speed was more nearly the same for the three impellers than the variation of slip factor and peak adiabatic efficiency. Impeller C had the highest pressure ratios at equivalent tip speeds as high as 1200 feet per second, impeller B had the highest at 1300 and 1500 feet per second, and impeller A had the highest at 1400 feet per second.

4. Impeller C had the highest maximum specific capacity at all equivalent tip speeds up to 1500 feet per second. Impeller B had nearly the same maximum specific capacity as impeller C and impeller A had a maximum specific capacity 6 to 11 percent smaller than that of impeller C.

5. Impeller B had the largest useful operating range at a pressure ratio of 1.80; impeller A had the largest useful operating range between pressure ratios of 2.20 to 3.00; and impeller C had the smallest useful operating range at all pressure ratios.

6. Impellers B and C exhibited an operational instability at high equivalent tip speeds near the maximum specific capacity.

Flight Propulsion Research Laboratory,
National Advisory Committee for Aeronautics,
Cleveland, Ohio, February 21, 1947.

REFERENCES

1. Ritter, William K., and Johnsen, Irving A.: Preliminary Investigation of Deep Inducers as Separate Supercharger Components. NACA ARR No. E5I28, 1945.

2. Ritter, William K., Ginsburg, Ambrose, and Boedo, William L.: Performance Comparison of Two Deep Inducers as Separate Components and in Combination with an Impeller. NACA ARR No. E5J03, 1945.

3. Ellerbrock, Herman H., Jr., and Goldstein, Arthur W.: Principles and Methods of Rating and Testing Centrifugal Superchargers. NACA ARR, Feb. 1942.

4. Hottle, H. C., and Kalitinsky, A.: Temperature Measurements in High-Velocity Air Streams. Jour. Appl. Mech., vol. 12, no. 1, March 1945, pp. A25-A32.

5. NACA Subcommittee on Supercharger Compressors: Standard Method of Graphical Presentation of Centrifugal Compressor Performance. NACA ARR No. E5F13a, 1945.

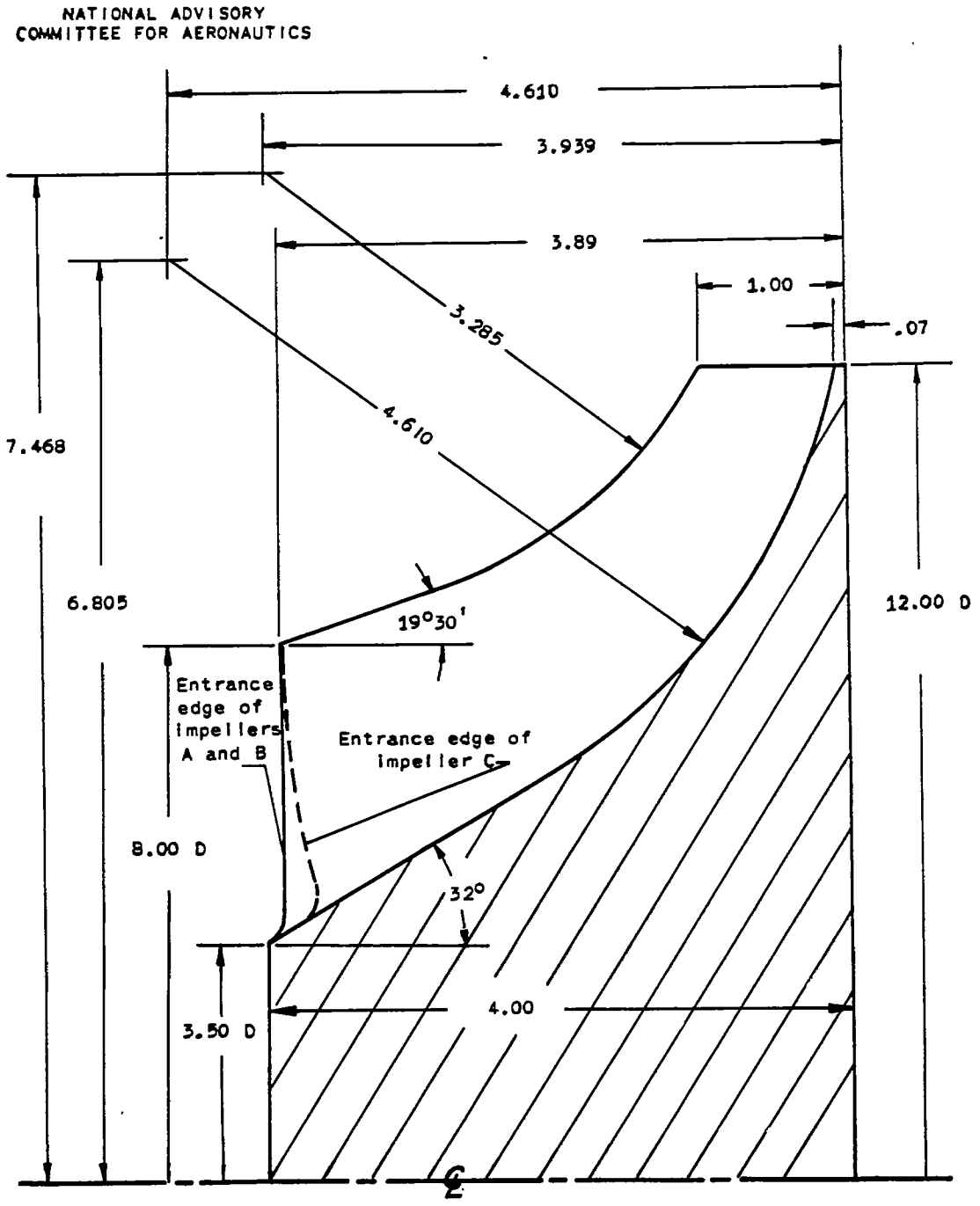

Figure 1. - Axial-plane section of impellers A, B, and C. All dimensions in inches.

(a) Impeller A, parabolic blading.

(b) Impeller B, elliptical blading.

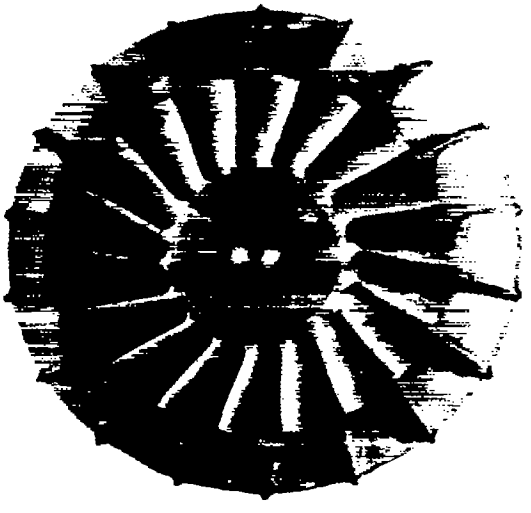

(c) Impeller C, circular blading.

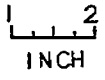

NACA
C-17855
2-12-47

Figure 2. - Front view of impellers.

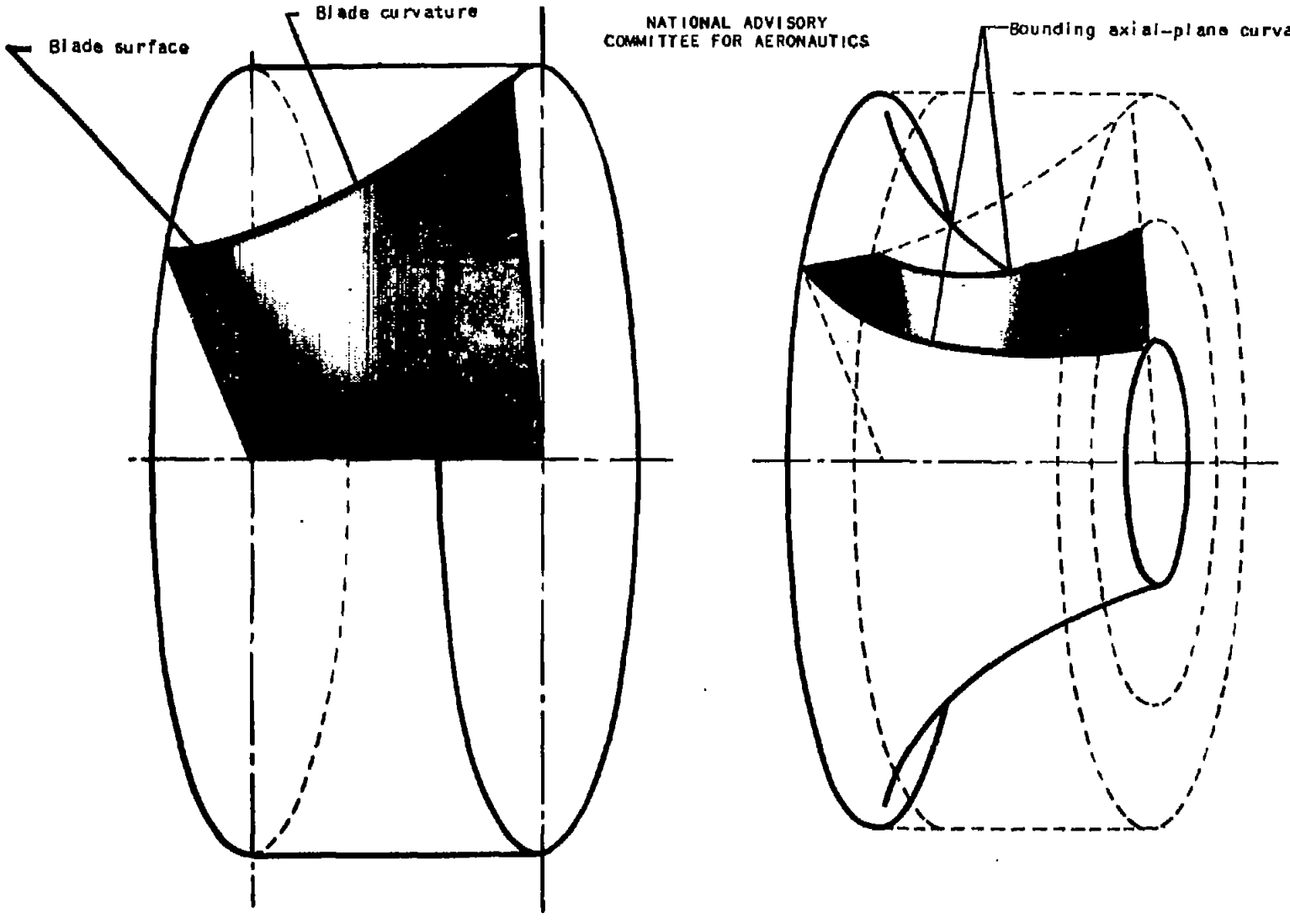

(a) Blade curvature on surface of cylinder.

(b) Portion of blade surface used by impeller.

Figure 3. - Relation of blade curvature to impeller A.

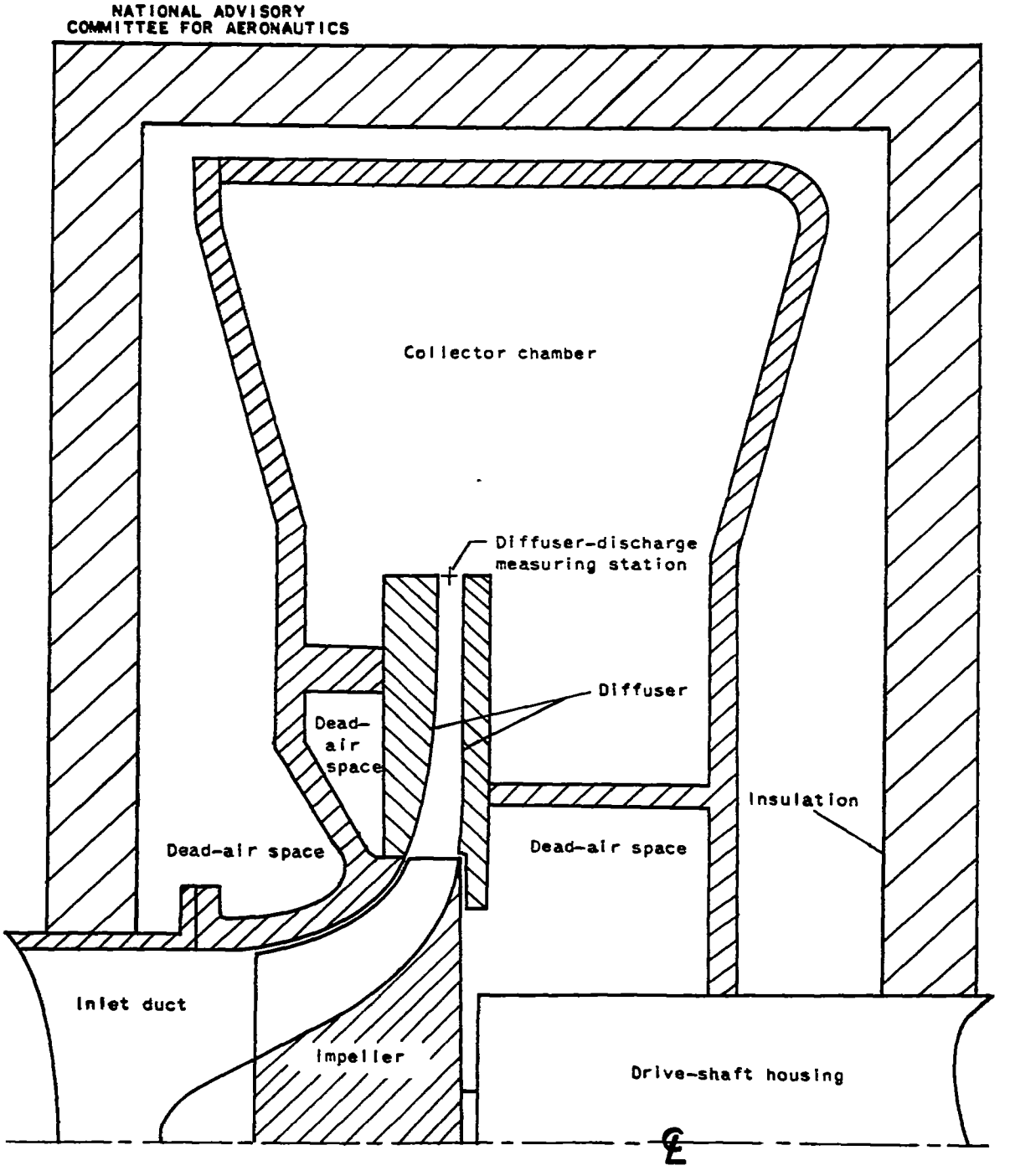

Figure 4. - Schematic view of compressor.

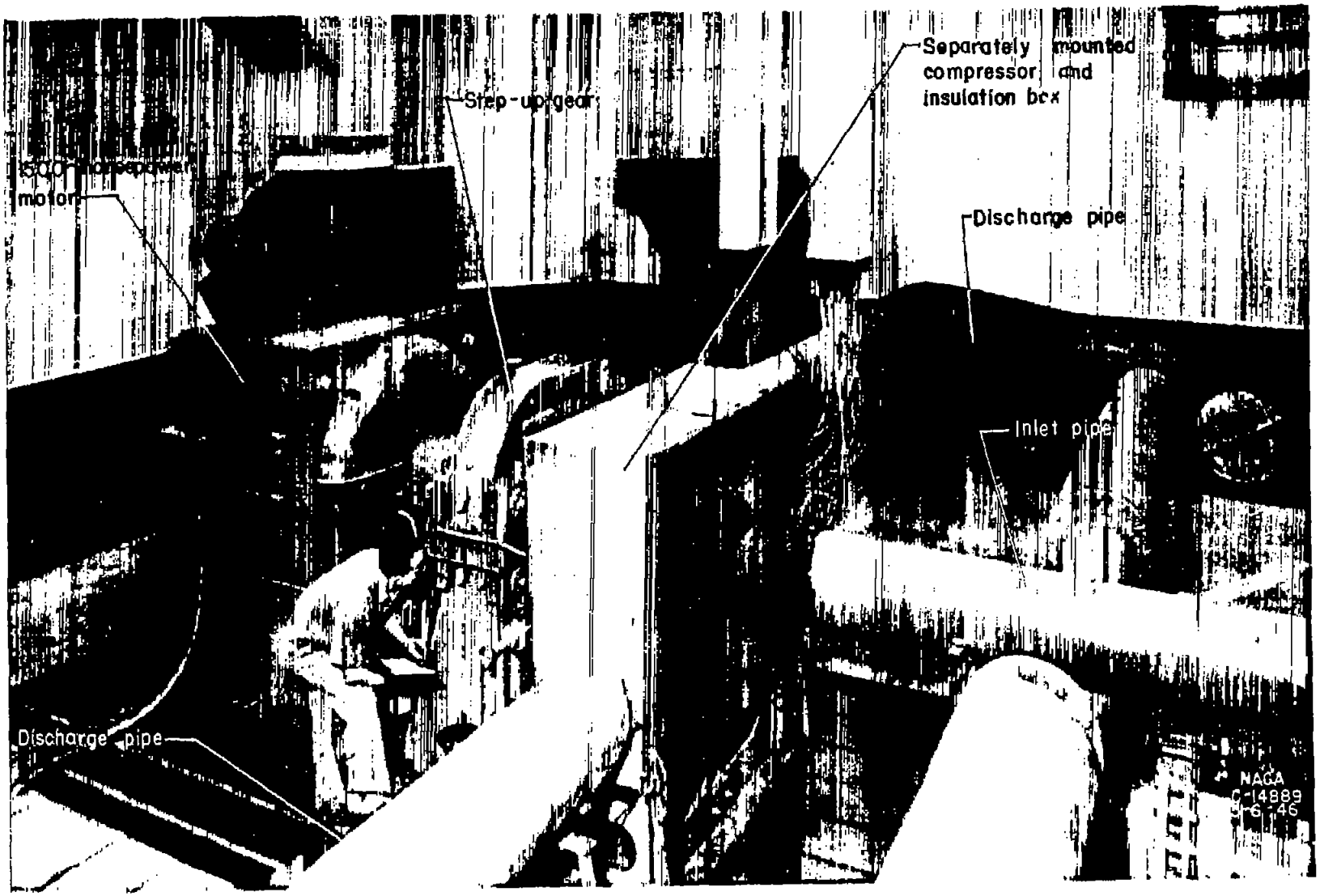

Figure 5. - Setup of equipment.

725

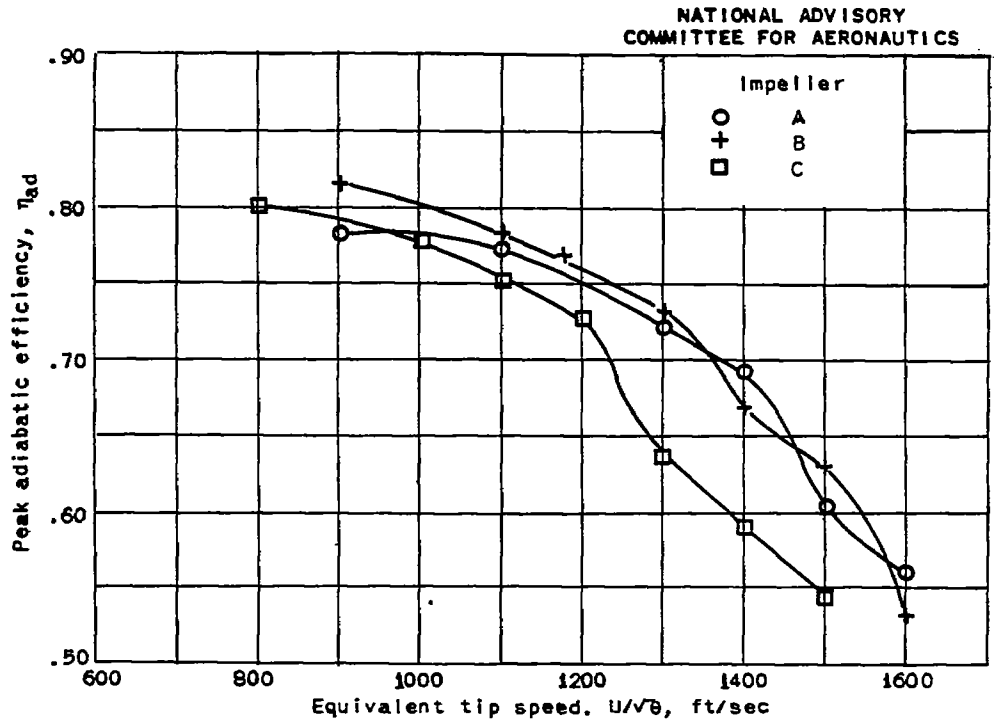

Figure 6. - Comparison of peak adiabatic efficiencies.

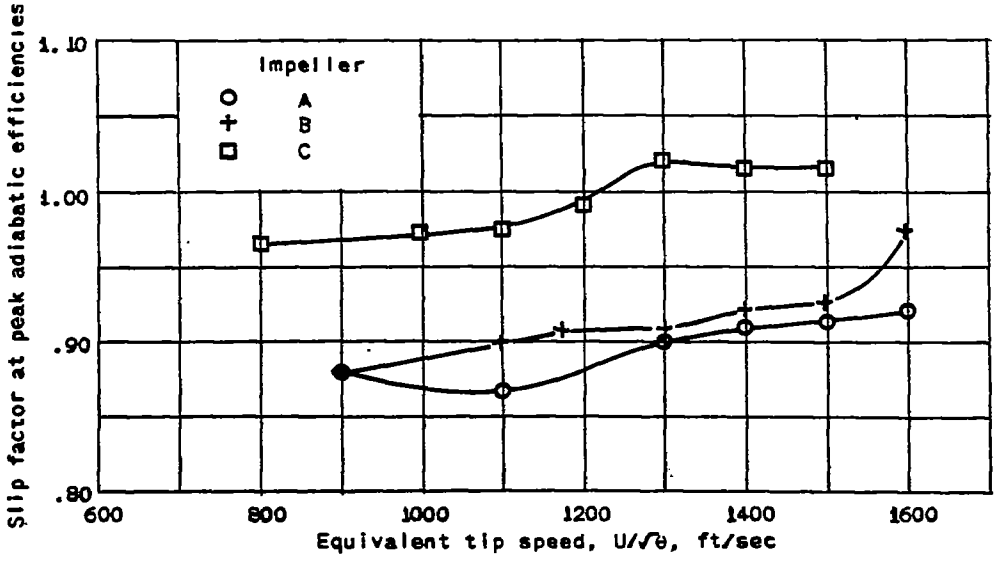

Figure 7. - Comparison of slip factors at peak adiabatic efficiency.

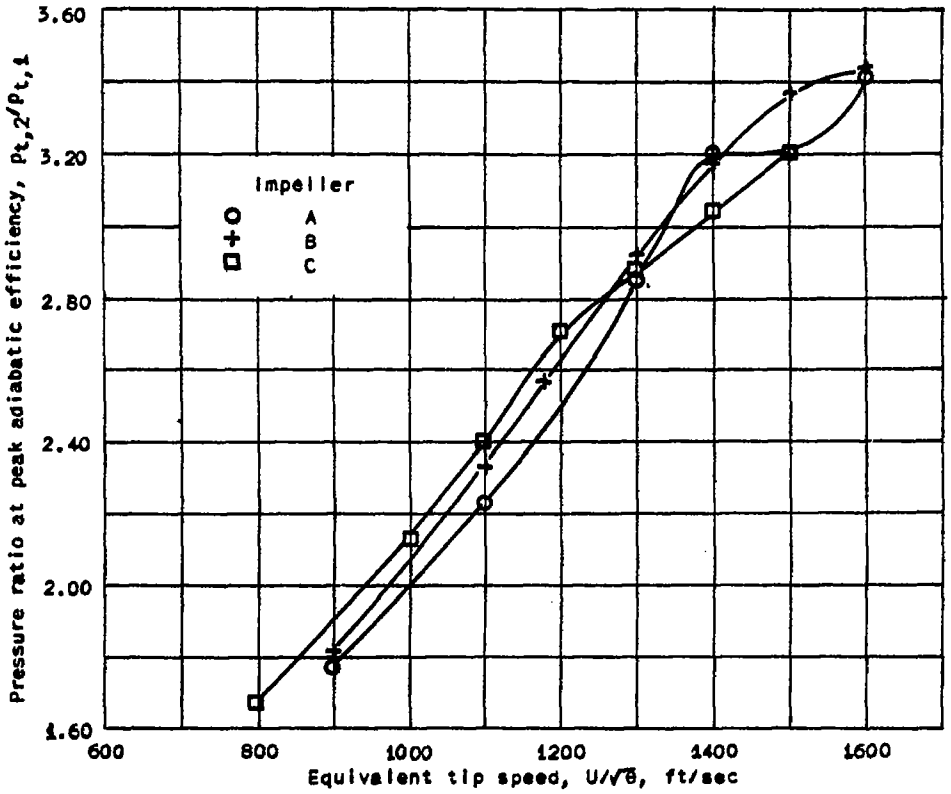

Figure 8. - Comparison of pressure ratios at peak adiabatic efficiency.

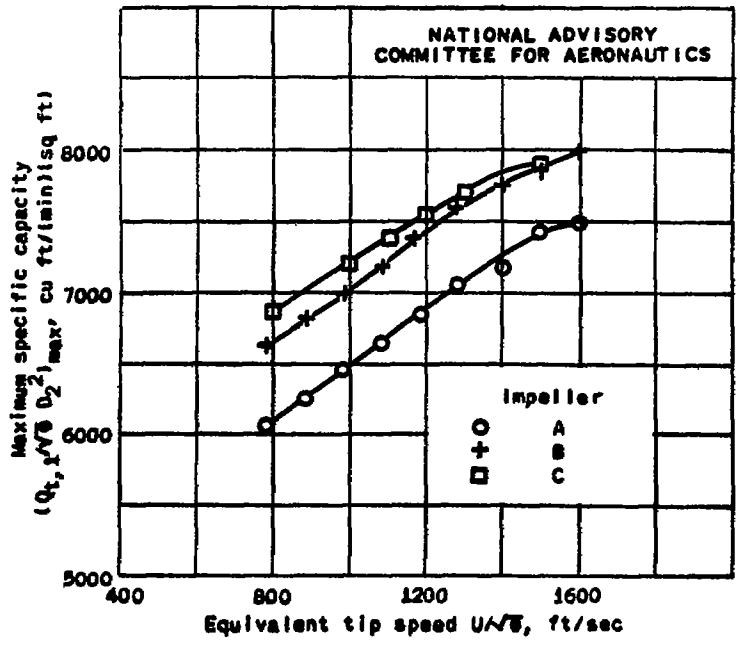

Figure 9. - Comparison of maximum specific capacity.

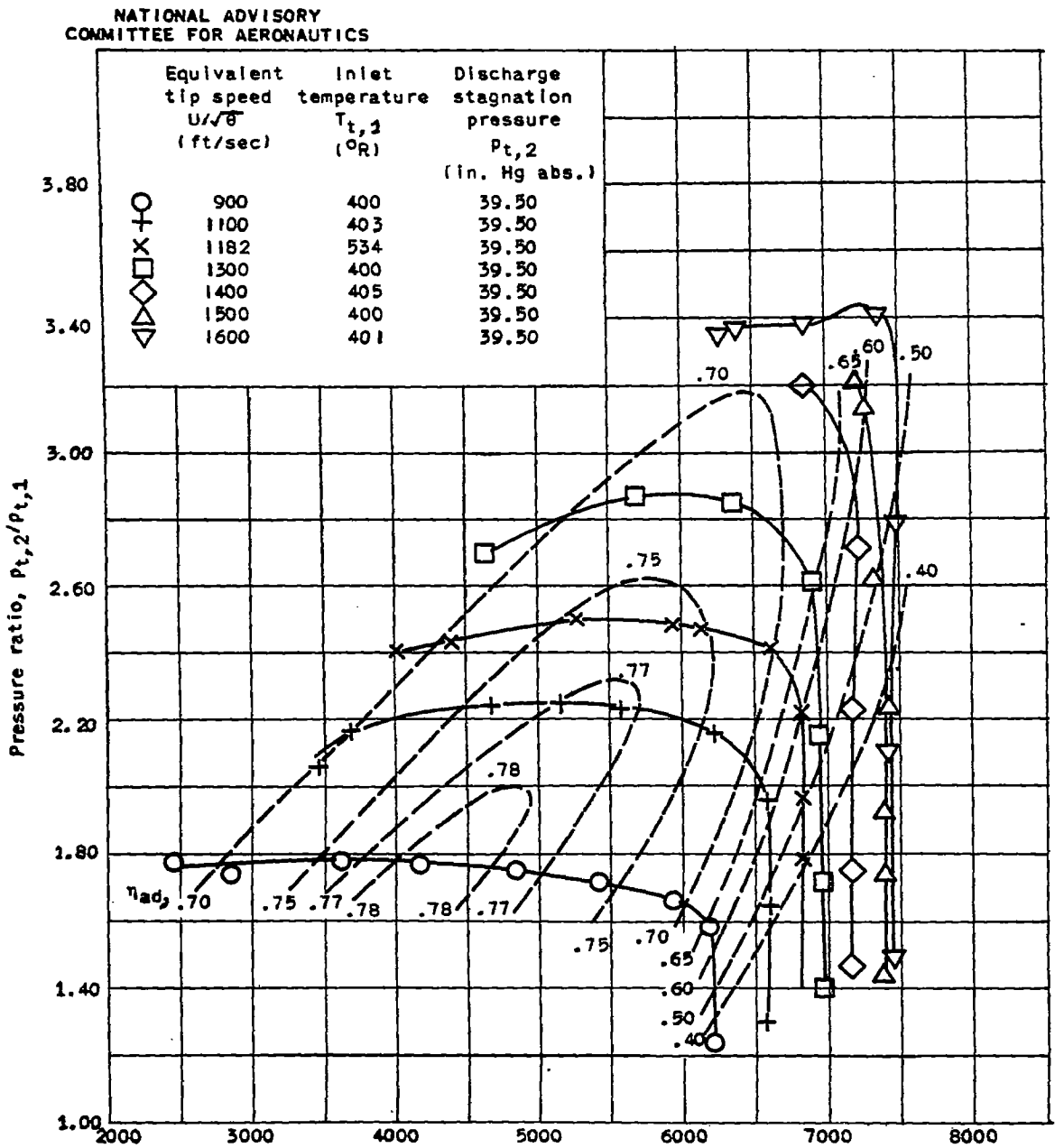

(a) Impeller A.

Figure 10. - Performance characteristics of impellers.

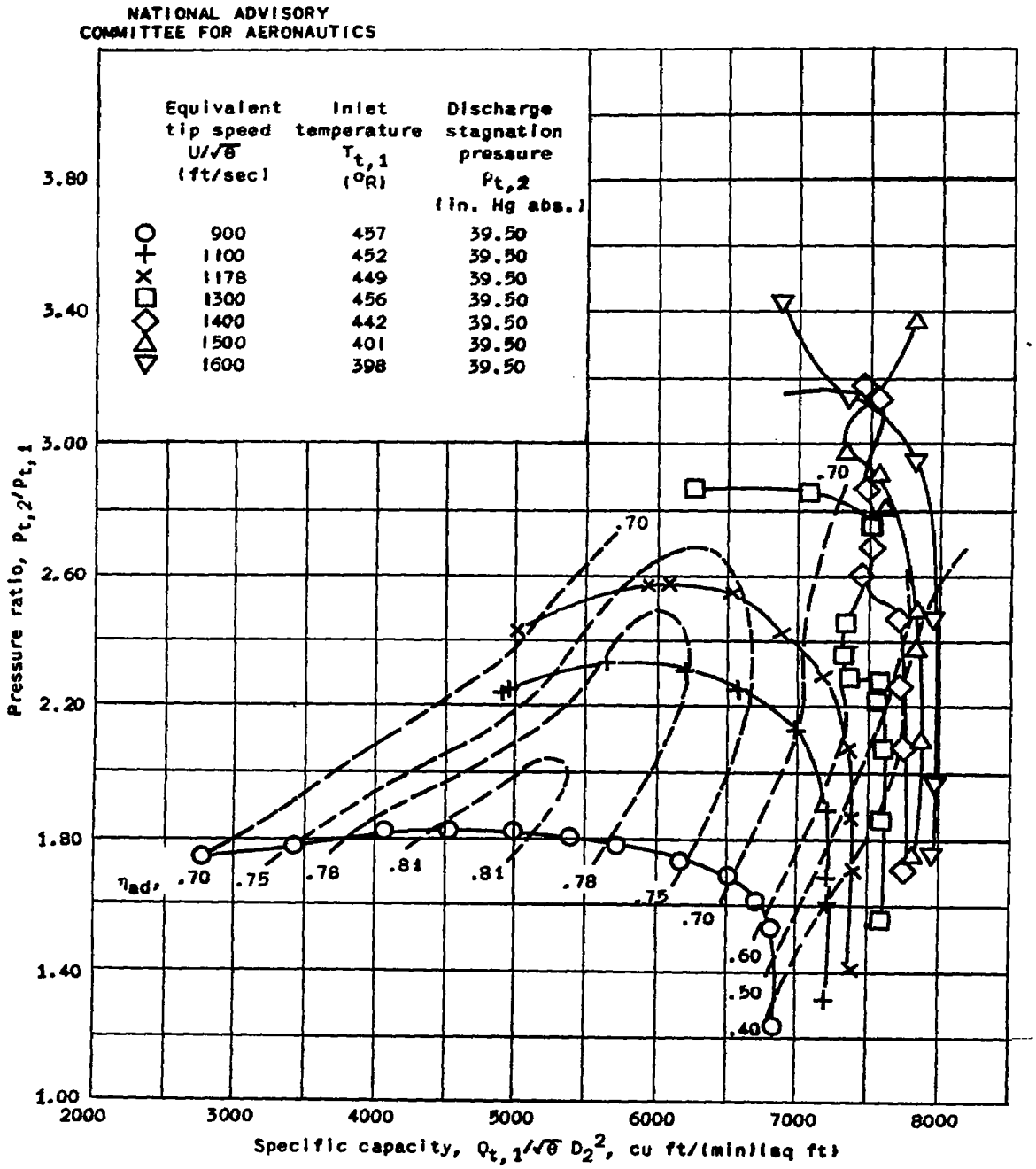

(b) Impeller B.

Figure 10. – Continued. Performance characteristics of impellers.

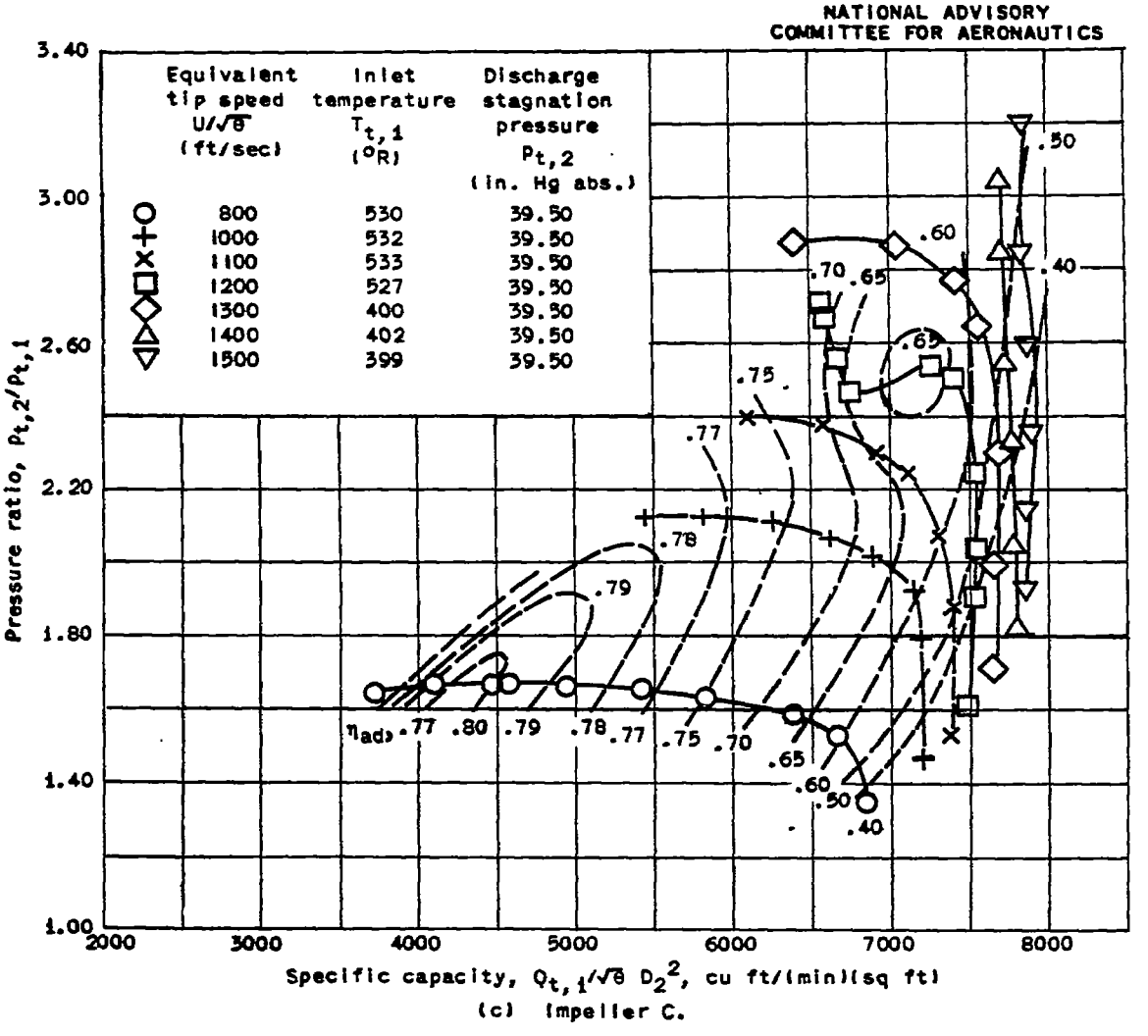

(c) Impeller C.

Figure 10. – Concluded. Performance characteristics of impellers.

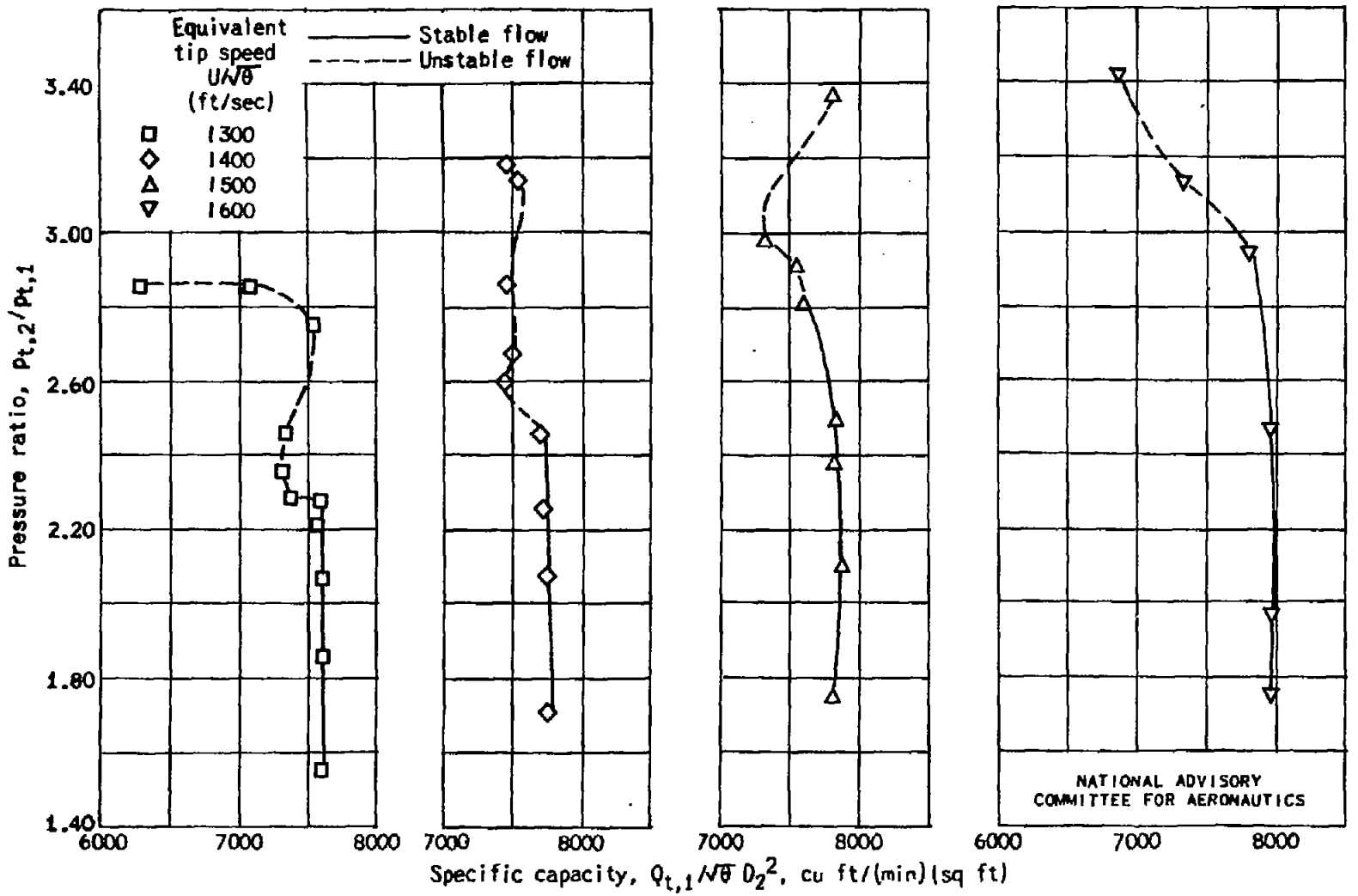

Figure 11. – High-speed performance characteristics of impeller B.

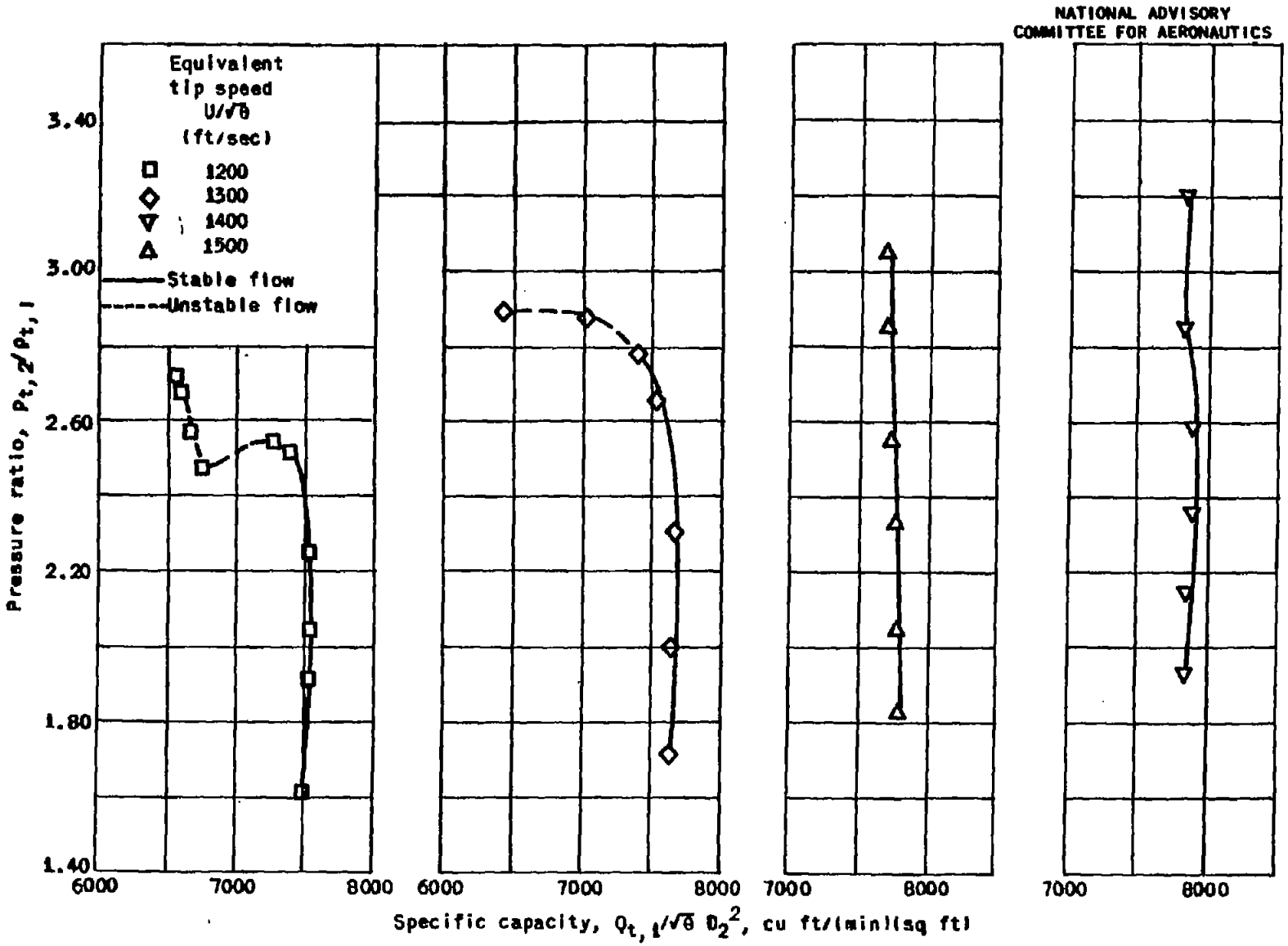

Figure 12. - High-speed performance characteristics of impeller C.